Structurally Sophisticated Octahedral Metal Complexes as Highly Selective Protein Kinase Inhibitors

15 AUTHORS, INCLUDING:

Klaus Harms
Philipps University of Marburg
693 PUBLICATIONS **9,597** CITATIONS

Stefan Knapp
University of Oxford
264 PUBLICATIONS **10,065** CITATIONS

Lars-Oliver Essen
Philipps University of Marburg
118 PUBLICATIONS **4,761** CITATIONS

Eric Meggers
University of Marburg & Xiamen University (s…
155 PUBLICATIONS **4,916** CITATIONS

Structurally Sophisticated Octahedral Metal Complexes as Highly Selective Protein Kinase Inhibitors

Li Feng[†], **Yann Geisselbrecht**[†], **Sebastian Blanck**[†], **Alexander Wilbuer**[†], **G. Ekin Atilla-Gokcumen**[†], **Panagis Filippakopoulos**[‡], **Katja Kräling**[†], **Mehmet Ali Celik**[†], **Klaus Harms**[†], **Jasna Maksimoska**[§], **Ronen Marmorstein**[§], **Gernot Frenking**[†], **Stefan Knapp**[‡], **Lars-Oliver Essen**[†], and **Eric Meggers**[†,*]

[†]Fachbereich Chemie, Philipps-Universität Marburg, Hans-Meerwein-Straße, 35043 Marburg, Germany

[‡]Structural Genomics Consortium, Oxford University, Old Road Campus Building, Roosevelt Drive, Oxford, OX3 7DQ, United Kingdom

[§]Department of Chemistry, University of Pennsylvania, 231 South 34th Street, Philadelphia, PA 19104, USA, and The Wistar Institute, 3601 Spruce Street, Philadelphia, PA, 19104, USA

Abstract

The generation of synthetic compounds with exclusive target specificity is an extraordinary challenge of molecular recognition and demands novel design strategies, in particular for large and homologous protein families such as protein kinases with more than 500 members. Simple organic molecules often do not reach the necessary sophistication to fulfill this task. Here, we present six carefully tailored, stable metal-containing compounds in which unique and defined molecular geometries with natural-product-like structural complexity are constructed around octahedral ruthenium(II) or iridium(III) metal centers. Each of the six reported metal compounds displays high selectivity for an individual protein kinase, namely GSK3α, PAK1, PIM1, DAPK1, MLCK, and FLT4. Although being conventional ATP-competitive inhibitors, the combination of the unusual globular shape and rigidity characteristics, of these compounds facilitates the design of highly selective protein kinase inhibitors. Unique structural features of the octahedral coordination geometry allow novel interactions with the glycine-rich loop, which contribute significantly to binding potencies and selectivities. The sensitive correlation between metal coordination sphere and inhibition properties suggests that in this design, the metal is located at a "hot spot" with the ATP binding pocket, not too close to the hinge region where globular space is unavailable, and at the same time not too far out towards the solvent where the octahedral coordination sphere would not have a significant impact on potency and selectivity. This study thus demonstrates that inert (stable) octahedral metal complexes are sophisticated structural scaffolds for the design of highly selective chemical probes.

Introduction

Biological and medicinal research relies on chemical reagents – often called "chemical probes" or "molecular probes" – that selectively modulate biomacromolecular functions.[1–3] Although selectivity is a key criterion for the usefulness of such probes,[4] the design of

compounds that reach this desired exclusive target selectivity is a truly extraordinary challenge of molecular recognition in view of the large number of different biomolecules in a cell in addition to the existence of large and homologous protein families.[5–11] Considering this situation, one might wonder whether the standard small organic molecules currently used in pharmacological research contain sufficient structural complexity and structural preorganization to achieve the desired protein binding selectivity.[12] Therefore, novel and creative strategies are needed for the design of highly target-specific bioactive compounds in order to more precisely control and manipulate biological processes.[13]

A few years ago we initiated a research program to use metal complexes as scaffolds for the design of enzyme inhibitors.[14] Metals such as Ru(II), Os(II), Rh(III), and Ir(III) are capable of forming highly stable complexes that expand on the limited coordination modes of carbon, thereby providing new opportunities for building small molecular geometries and thus populating unique regions of chemical space that cannot be explored with purely organic compounds.[15–17] After spending considerable time evaluating organometallic half-sandwich structures as scaffolds for the design of enzyme inhibitors,[14] we recently became particularly intrigued by the structural opportunities offered by truly octahedral coordination geometries.[18–20] Strikingly, an octahedral geometry permits much larger structural complexity compared to, for example, a tetrahedral binding mode. This can simply be illustrated by the number of possible stereoisomers: whereas a tetrahedral center is capable of building a maximum of two enantiomers, an octahedral center can form up to 30 stereoisomers.[15,16] Furthermore, an octahedral coordination sphere simplifies the design of small globular and rigid structures because molecular geometries are basically constructed from a single center with chelating ligands limiting the degree of conformational flexibility.[19] Thus, in such stable octahedral metal complexes, the metal can be considered as a virtually hypervalent carbon providing untapped opportunities for the design of novel globular, well-defined molecular structures which populate previously inaccessible regions of chemical space.[21]

As a proof of concept, the strategy of using inert metals as templates for defining the structure of small molecules was applied to the design of protein kinase inhibitors and we utilized the natural product staurosporine as an inspiration for pyridocarbazole metal complexes (Figure 1).[14] This scaffold binds to the ATP binding site of protein kinases with the pyridocarbazole moiety occupying the adenine pocket (Figure 1b) and the remaining metal complex fragment with additional ligands A-D filling the ribose triphosphate binding site. Building on our extensive previous work on structurally simplified metallo-pyridocarbazole half sandwich complexes (A, B, C = $\eta^5-C_5H_5$ or $\eta^6-C_6H_6$),[14,22,23] we demonstrate here that truly octahedral pyridocarbazole metal complexes, dubbed octasporines (**OS**), are privileged scaffolds for the design of highly selective protein kinase inhibitors, being superior to canonical organic structures.

Results

We started by selecting a panel of six diverse protein kinases, namely GSK3α, PIM1, PAK1, DAPK1, MLCK (also known as MYLK), and FLT4 (also known as VEGFR3) as our targets for developing highly selective protein kinase inhibitors. These kinases were identified as suitable targets for the octasporine scaffold based on previous work (GSK3α,[18] PIM1,[18] PAK1,[19] FLT4[20]) and unpublished results (DAPK1, MLCK). Our goal was to create highly selective metal-based inhibitors for each of these protein kinases by exploiting different octahedral coordination spheres occupying the ATP binding site. Accordingly, Figure 2 illustrates six octasporine derivatives **OS1–OS6** that were developed utilizing structure-based design, combinatorial chemistry, standard structure-activity-relationships, and combinations thereof.

A common feature of all six complexes is the designed hinge-binding pyridocarbazole chelate ligand coordinated to an octahedral metal center, which is either ruthenium or iridium. The complexes differ in their substituents at the pyridocarbazole heterocycle and the nature of the additional ligands that complete the octahedral metal coordination sphere. These range from monodentate ligands, such as CO, thiocyanate, azide, selenocyanate, chloride, and methyl to bidentate ligands, such as 2-aminomethylpyridine, 2-phenyliminomethyl-4-aminopyridine, and dibenzo[*a,e*]cyclooctatetraene, and even tridentate ligands such as 1,4,7-trithiacyclononane and its monosulfoxide derivative. All complexes contain defined relative metal-centered stereochemistries with **OS1** and **OS2** used as single Λ-enantiomers (Λ-**OS1**, Λ-**OS2**) whereas **OS3–OS6** were used as racemic mixtures in this study. Some of the complexes are structurally highly complicated as indicated by the number of theoretically possible metal-centered stereoisomers. For example, whereas **OS3** and **OS4** can only form two enantiomers due to the high symmetry of the 1,4,7-trithiacyclononane ligand, **OS5** forms 6 stereoisomers, **OS6** forms 10 stereoisomers, and **OS1** and **OS2** can theoretically form up to 20 stereoisomers (10 diastereomers as pairs of enantiomers).

Although all six complexes contain ligands built around the same canonical octasporine scaffold, they exhibit diverse protein kinase inhibition profiles as shown in Table 1. For example, the ruthenium complex Λ-**OS1** was developed as a selective inhibitor for the a-isoform of glycogen synthase kinase 3 (GSK3α). Λ-**OS1** displays an IC$_{50}$ value of 0.9 nM at an ATP concentration of 100 μM and a selectivity of 15.6 to > 111000 fold in our small panel of six protein kinases. This compound differs from a previously reported and related complex by an additional amino substituent on the pyridocarbazole moiety.[18] This introduced substituent increases the affinity of Λ-**OS1** for GSK3α by one order of magnitude. To test its broader selectivity, we screened Λ-**OS1** at a concentration of 10 nM (10 μM ATP) against every human wild-type protein kinase in the Millipore KinaseProfiler panel that was used in the assay at a concentration that was equal or lower than the concentration of Λ-**OS1**, which covered 102 protein kinases. Strikingly, 98 out of the 102 kinases in this panel showed an activity higher than 75% under these conditions, whereas GSK3α displayed a residual activity of only 6%. The only kinases also significantly inhibited by this compound at 10 nM were PIM1 (13%, IC$_{50}$ = 14 nM, 100 μM ATP, Table 1), CLK2 (33%), and GSK3β (58%) (Figure 3a). Thus, it can be concluded that within the tested panel, Λ-**OS1** is a selective inhibitor of GSK3α.

In order to better understand the exact binding mode of Λ-**OS1** to GSK3, we expressed, purified, and crystallized full-length human GSK3β, as described recently,[23] and then soaked crystals with a solution of enantiomerically pure Λ-**OS1**. The structure of the complex was determined and refined to a resolution of 3.0 Å (Table 2). The overall structure revealed the typical two-lobe protein kinase architecture,[24] connected by the so-called hinge region, with the catalytic site positioned in a deep intervening cleft and Λ-**OS1** occupying the ATP-binding site, similar to the binding mode of staurosporine and many other synthetic ATP-mimetic organic inhibitors (Figure 4a).[25,26] The maleimide moiety of Λ-**OS1** forms two canonical hydrogen bonds with the hinge region by donating a hydrogen bond from the maleimide NH to the backbone amide carbonyl group of Asp133 (2.9 Å) and accepting a hydrogen bond from the backbone amide NH group of Val135 (2.7 Å) to one of the maleimide carbonyl groups (Figure 4b). Furthermore, the NH$_2$-substituent at the pyridine moiety is in hydrogen bonding distance with the backbone carbonyl groups of Val135 (3.3 Å) and Pro136 (3.1 Å). Together, the binding of Λ-**OS1** to GSK3β is stabilized by 3–4 hydrogen bonds to the hinge region. The pyridocarbazole heterocycle is sandwiched by key hydrophobic contacts from amino acids of the N-terminal (Ile62, Phe67, Val70, Ala83, Lys85, Val110) and C-terminal (Leu132, Glu137, Thr138, Leu188, Cys199, Asp200) domains together with Tyr134 and Val135 of the hinge region. The 2-aminomethylpyridine

ligand undergoes edge-to-face stacking with Phe67 and the coordinated NH_2-group forms a hydrogen bond with the backbone carbonyl group of Gln185 (2.9 Å) (Figure 4b,c). Most interestingly, the ruthenium-coordinated CO ligand interacts extensively with the flexible glycine-rich loop[27,28] exploiting by induced fit a small hydrophobic pocket formed by Ile62, Gly63, Phe67 and Val70. This pocket perfectly accommodates the small hydrophobic CO axial ligand. It is noteworthy that the related natural product staurosporine cannot benefit from such strong hydrophobic interactions as exemplified by Phe67 which is rotated out towards the solvent in the complex with staurosporine (Figure 4d). The same unusual interaction between coordinated CO and the glycine-rich loop of GSK3β has been observed with related CO-containing half-sandwich complexes.[23,29] Since we have not observed any highly potent ruthenium-based inhibitors for GSK3 lacking this CO ligand, we conclude that this interaction with the flexible glycine-rich loop is a crucial driving force for binding potency and selectivity to GSK3. However, this structure does not provide any insight into the observed selectivity of Λ-**OS1** for the α- over β-isoform of GSK3 (ca. 7-fold, GSK3β: $IC_{50} = 6$ nM at 100 μM ATP), since all amino acid residues responsible for Λ-**OS1** binding are identical in both isoforms. One can hypothesize that the rigid ruthenium complex can distinguish between the two isoforms based on dynamic effects resulting from sequence differences at more distal sites.

Interestingly, starting from the GSK3α inhibitor Λ-**OS1** and introducing just a few modifications at the periphery, such as changing the substitution pattern and orientation of the pyridocarbazole moiety and replacing the aminomethylpyridine for a more bulky iminopyridine ligand, the compound Λ-**OS2** is derived, which exhibits a switched selectivity in favor of PAK1 over GSK3α (Figure 2 and Table 1). This is a remarkable observation since Λ-**OS1** does not detectably inhibit PAK1 ($IC_{50} > 100000$ nM) which translates to a change of the IC_{50} value ratio of GSK3α/PAK1 by 5 orders of magnitude, going from Λ-**OS1** (ratio < 0.000009) to Λ-**OS2** (ratio = 5.7). PAK1 has a very open active site and can accommodate the bulky and rigid complex Λ-**OS2** as opposed to most other protein kinases.[19] Replacing the bulky iminopyridine ligand together with the chloride for a tridentate cyclic 1,4,7-trithiacyclononane ligand, in addition to some variation at the pyridocarbazole moiety, afforded the octasporine complex **OS3** (racemic) which displayed a switched selectivity profile with a sub-nanomolar IC_{50} value for the protein kinase PIM1 ($IC_{50} = 0.075$ nM at 100 μM ATP) and at the same time a selectivity over PAK1 and GSK3α of 1093-times and 267-times, respectively.

All compounds discussed so far, Λ-**OS1**, Λ-**OS2**, and **OS3**, contain a monodentate axial CO ligand which is oriented perpendicular to the pyridocarbazole moiety and thereby interacts with the flexible glycine-rich loop as revealed by the interaction of Λ-**OS1** with GSK3 but also revealed in multiple other co-crystal structures of CO-containing metal complexes with protein kinases.[19,23,29,30] We speculated that pointing other monodentate ligands towards the glycine-rich loop might have significant effects on the binding potencies and selectivities of this class of compounds. Indeed, starting from the 1,4,7-trithiacyclononane scaffold **OS3** and replacing the axial CO for a thiocyanate ligand, in addition to some modifications at the pyridocarbazole moiety, afforded complex **OS4** (racemic) with a switched selectivity profile now in favor of the protein kinase DAPK1, with an IC_{50} value of 2.0 nM (100 μM ATP) and an 85-fold selectivity over PIM1. Interestingly, the protein kinases GSK3α and PAK1 were not detectably inhibited by this compound ($IC_{50} > 100$ μM). Figure 3b summarizes the screening results of **OS4** at a concentration of 10 nM (10 μM ATP) against every human wild-type protein kinase in the Millipore KinaseProfiler panel that was used in the assay at a concentration of 10 nM or less (102 protein kinases). As a result, 96 out of the 102 kinases in this panel showed an activity higher than 60%, compared to DAPK1 which displayed a residual activity of only 12% under these conditions and the remaining kinases being ZIPK (22%), RSK2 (27%), RSK1 (31%), MELK (37%), and PIM1 (38%, see Table 1 for IC_{50}).

We verified the IC_{50} value of **OS4** against ZIPK to be 8.8 nM at 100 μM ATP. Therefore, it can be concluded that **OS4** is selective for DAPK1 in this panel of 102 protein kinases with a selectivity factor of at least 4.4.

In order to better understand the binding mode of **OS4** to DAPK1, we expressed, purified, and co-crystallized DAPK1 with racemic **OS4**, then solved and refined the structure to a resolution of 2.2 Å (Table 2). The overall fold is shown in Figure 5a and reveals that the (R)-enantiomer of **OS4** occupies the ATP-binding site. In analogy to Λ-**OS1**, the maleimide moiety of (R)-**OS4** forms two canonical hydrogen bonds with the hinge region of DAPK1 (Glu94 and Val96) (Figure 5b). In addition, the isopropyl ether oxygen of the indole moiety is in hydrogen bonding distance to a water molecule (2.7 Å), which is held in place by three additional hydrogen bonds to amino acids Lys42 (3.0 Å), Glu64 (2.8 Å), and Asp161 (2.5 Å) (Figure 5b,c). The pyridocarbazole heterocycle is sandwiched by key hydrophobic contacts from amino acids of the N-terminal (Leu19, Val27, Ala40, Ile77, Leu93) and C-terminal (Met146, Ile160) domains together with Val96 of the hinge region (Figure 5b). The isopropyl substituent reaches into a small hydrophobic pocket created by Lys42, Leu68, Ile77, Leu91, Leu93, and Ile160, whereas the 1,4,7-trithiacyclononane ligand points towards the more hydrophilic entrance of the ATP-binding site with the most important hydrophobic interactions to Glu143, Met146, and Ile160, but also to Gly20 and Ser21 of the glycine-rich loop. The NCS ligand occupying the metal axial position is coordinated in a slightly bent fashion (Ru-N-C = 143°) and points towards the flexible glycine-rich loop, resulting in close contact with the side chain residues of Ala25, Val27, and Lys42, as well as the backbone residues of Gly20, Ser21, and Val26 (Figure 5c). Interestingly, in a small molecule crystal structure of a compound closely related to **OS4**, the NCS ligand is coordinated in a more linear fashion (Ru-N-C = 172°) (see Supporting Information). Density functional theory (DFT) calculations reveal that the energy differences between the straight and bent coordination mode is only modest (see Supporting Information), implying that the binding angle of the NCS ligand can adjust to the geometry necessary for an optimal interaction with the glycine-rich loop. The steric demand of this axial substituent induces a more open conformation of the glycine-rich loop when compared to a DAPK1 structure in complex with the nonhydrolyzable ATP analog AMPPnP (Figure 5d).[31] It is noteworthy that the glycine-rich loop of DAPK1 is much more "stretched out" compared to the glycine-rich loop of GSK3β (Figure 4d) and other protein kinases, a conformation that generates a hydrophobic pocket that closely matches the shape of the NCS ligand, whereas the smaller pocket formed by the glycine-rich loop of GSK3 is better matched by the smaller and linear CO axial ligand. Taken together, the selectivity data presented here in combination with the protein crystal structures suggest that selectivity for protein kinases can be tuned significantly by tailored interactions with the glycine-rich loop, a surprising and unique finding given that this region is known to be rather flexible in protein kinases.

Using **OS4** as a starting point and replacing the thiocyanate ligand for an azide, removing the fluorine, and oxidizing one thioether ligand to its sulfoxide, leads to the related complex **OS5** (racemic) which again displays a switched inhibition profile, with high selectivity for MLCK (IC_{50} = 4.4 nM). Despite the high structural similarity between **OS4** and **OS5**, **OS5** displayed an 26-fold selectivity for MLCK over DAPK1, switched from 12.5-fold in favor of DAPK1 over MLCK for **OS4**. In order to evaluate its global selectivity profile, we screened **OS5** at a concentration of 100 nM against 191 protein kinases (all wild type human protein kinases in the Millipore KinaseProfiler which are used in the assay at a concentration ≤ 100 nM). The resulting data presented in Figure 3c revealed that 145 out of the 191 kinases were more than 50% active under these conditions whereas MLCK showed a residual activity of only 3% under these conditions (10 μM ATP). No other kinases are inhibited more potently with Ret (3%), ZIPK (4%), and DAPK1 (6%) being the next most inhibited kinases in this panel. Subsequent inhibition measurements revealed that these

kinases exhibit higher IC_{50} values than MLCK (IC_{50} values at 100 μM ATP: Ret = 70 nM, ZIPK = 18 nM, DAPK1 = 113 nM), thus demonstrating the high selectivity of the MLCK inhibitor **OS5**.

Finally, based on a recently discovered iridium complex scaffold,[20] we developed the octahedral iridium complex **OS6** as a highly selective inhibitor for the receptor tyrosine kinase FLT4 (also known as VEGFR3). In this complex, iridium in the oxidation state +3 is coordinated octahedrally to one pyridocarbazole moiety in addition to a CH_3, a selenocyanate, and a bidentate dibenzo[*a,e*]cyclooctatetraene ligand. **OS6** displayed an IC_{50} value of 42 nM (100 μM ATP, Table 1) against FLT4 with a respectable selectivity of 8-fold to more than 2380-fold over the other kinases listed in Table 1. The impressive selectivity of this compound was further demonstrated by screening it against a panel of 215 human wild-type protein kinases at a concentration of 300 nM (10 μM ATP). As in all other assays, the protein kinases were selected solely on the basis of their assay concentration (≤ the inhibitor concentration of **OS6**). As a result, as shown in Figure 3d, 203 out of 215 kinases displayed activities of > 50% at 300 nM **OS6**, whereas FLT4 was the most potently inhibited target to just 6% of residual activity. Interestingly, the closely related protein kinases FLT1 (also known as VEGFR1) (12%, determined IC_{50} = 151 nM at 100 μM ATP), FLT3 (26%), and KDR (also known as VEGFR2) (56%) were inhibited more weakly. Thus, **OS6** is a highly selective FLT4 inhibitor which can even significantly distinguish between VEGFR isoforms. We believe that this high selectivity is the consequence of the scaffold rigidity combined with its large size that almost fills the complete ATP binding site, thus rendering the inhibitor very sensitive to even small structural differences.

Discussion

For the design and discovery of compounds with desired biological properties, chemical biology and medicinal chemistry rely predominately on organic molecules. Organic chemistry provides without any dispute extremely powerful tools for building diverse and complicated structures. However, it is also apparent that the construction of organic molecules, which are globular and structurally highly preorganized, requires sophisticated and complicated scaffolds that are typically synthetically not accessible in a straightforward fashion. A recent study investigated the protein binding properties of compounds from natural and synthetic sources and found that protein binding selectivity correlates with shape complexity (defined as the relative content of sp^3-hybridized carbons) and stereochemical complexity (defined as the relative content of stereogenic carbons).[32] In this respect, octahedral metal complexes may offer an attractive alternative strategy for constructing complicated "natural-product-like" three dimensional structures with unique and defined shapes and hitherto unprecedented properties. All six octahedral metal-based kinase inhibitors developed in this study display very defined globular, relatively rigid shapes and distinguished electrostatic potential surfaces, as mapped with a color code on electron density isosurfaces in Figure 6. It is intriguing how sensitive the binding properties of the individual metal complexes depend on the exact ligand sphere around the metal center. Apparently, in our octasporine design, the metal is located at a "hot spot" within the ATP binding pocket, not too far inside towards the hinge region, where globular space is not available, and at the same time not too far out towards the solvent where the octahedral coordination sphere would not have a significant impact on potency and selectivity.[33] We conclude that the combination of globular space requirement and high rigidity facilitate the design of highly selective protein kinase inhibitors.

Although the octahedral metal complexes presented in this work are conventional ATP-competitive binders, their unique shapes allow novel interactions with the glycine-rich loop of protein kinases which appears to be a crucial factor for binding potency and selectivity.

We are not aware of other examples of selectivity-determining noncovalent interactions between the glycine-rich loop and purely organic protein kinase inhibitors. A special and unique feature of the octahedral metal center in the octasporine scaffold is its ability to present a ligand directly perpendicular to the heterocyclic pyridocarbazole hinge binder as indicated in Figure 1b, thus pointing functional groups directly towards the glycine rich loop, a feature which can be further used to exploit differences in the conformations of this loop and the relative position to the hinge region as seen in the superimposed GSK3β/Λ-**OS1** and DAPK1/(*R*)-**OS4** structures (Figure 7). Such interactions between inhibitor and the glycine-rich loop of protein kinases constitute a novel strategy for achieving protein kinase selectivity.

Conclusions

In conclusion, we presented here a detailed study on the protein kinase binding and selectivity properties of carefully tailored octahedral metal complexes. The octahedral metal centers provide the opportunity to generate structures with natural-product-like shape and stereochemical complexity in a straightforward fashion. The globular and rigid nature of these complexes in combination with a well positioned metal center within the ATP binding site allows selectivity-determining interactions with the glycine-rich loop. Therefore, although these octasporines are conventional ATP-competitive binders, they display exquisite selectivities and will serve as powerful chemical probes for deciphering kinase activity and understanding cellular signalling.

Experimental Part

Synthesis and characterization of Λ-OS1, Λ-OS2 and OS3-OS6

A detailed description of the synthesis and characterization of these compounds is given in the Supporting Information.

Selectivity profiles using protein kinase panels

Percentage kinase activities of octasporine inhibitors each at a single concentration (Λ-**OS1** = 10 nM, **OS4** = 10 nM, **OS5** = 100 nM, **OS6** = 300 nM) in panels of human wild type protein kinases were determined by KinaseProfiler™ (Millipore UK Ltd). Measurements were performed in duplicate and the average was taken. Protein kinases were selected from the Millipore KinaseProfiler™ panel solely based on the concentration of the protein kinase used in the assay so that the kinase concentration is equal to or lower than the concentration of the inhibitor (Λ-**OS1** and **OS4** = 102 kinases, **OS5** = 191 kinases, **OS6** = 215 kinases).

Protein kinase activity assays

The PAK1 kinase domain (residues 249 to 545) was expressed and purified as previously described.[19] All other kinases (human) and substrates were purchased from Millipore or MoBiTec GmbH. IC_{50} values were obtained by a conventional radioactive assay in which kinase activity was measured by the degree of phosphorylation of a substrate with [γ-^{33}P]ATP (Perkin Elmer). Accordingly, different concentrations of the inhibitors were preincubated with protein kinases in 20 mM MOPS pH 7.0, 30 mM $MgCl_2$, 0.8 μg/μL bovine serum albumin (BSA) and 5 % DMSO (resulting from the inhibitor stock solution) in the presence of substrates for 15 minutes, except for FLT4 and FLT1 which were incubated for 45 minutes. Reactions were initiated by adding ATP to a final concentration of 100 μM including [γ-^{33}P]ATP in a final volume of 25 μL. After incubation for a period of time, the reactions were terminated by spotting 17.5 μL onto circular P81 phosphocellulose paper (diameter 2.1 cm, Whatman), followed by washing three times with 0.75% phosphoric acid and one time with acetone. The dried P81 papers were transferred to scintillation vials and 5

ml of scintillation cocktail were added. The counts per minute (CPM) were measured with a Beckmann Coulter™ LS6500 Multi Purpose Scintillation Counter and the IC_{50} values were defined to be the concentration of inhibitor at which the counts per minute were 50% of the control sample, corrected by the background CPM. Specifics for each kinase and ligand used are given in Table 3.

Expression, purification and crystallization of the catalytic domain of human DAPK1

DH10B TonA cells transformed with pCR-XL-TOPO plasmid containing cDNA of human DAPK1 (accession number: BC113660) was purchased from Open Biosystems. Sterile LB media (50 mL) was inoculated with 5 μL of DH10B TonA cells and grown overnight. The plasmid was isolated the following day with a MidiPrep kit (Qiagen). The sequence corresponding to the catalytic domain of human DAPK1 (amino acids 1–285) was amplified by PCR from a plasmid using suitable primers and ligated into a pET151 vector (Champion™ pET-151 Directional TOPO Expression kit, Invitrogen) (Forward primer: 5'-CACCATGACCGTGTTCAGGCAGGAAAACGTG-3'; reverse primer: 5'-TCAACTAAGTGCCTGTTGTGTATCTTTAGG-3'). Protein production was carried out in *E. coli* Rosetta2-DE3 cells (Novagen). Cells were grown at 37 °C until they reached an O.D. = 0.6, then the temperature was reduced to 17 °C and protein expression was induced by the addition of 1 mM IPTG. Cells were allowed to grow for 4 hours, then were harvested and stored at −80 °C until further use.

Frozen cell pellets were thawed and resuspended in 50 mM HEPES pH 7.2, 300 mM NaCl, 10% glycerol, 1 μg/ml PMSF. Cells were lysed by sonication on ice for 3 minutes (in 3 intervals). After spinning (30 min at $42,500 \times g$), the supernatant was collected and loaded to a Ni-NTA column (Qiagen). The column was washed with 10 mM and 50 mM imidazole containing 50 mM HEPES pH 7.2, 300 mM NaCl, 10% glycerol followed by the elution of the protein with a gradient of 10 to 250 mM imidazole containing buffer. The solution was diluted with 50 mM HEPES pH 7.2, 10% glycerol, 20 mM DTT, 4 mM $MnCl_2$. In order to cleave the N-terminal fusion tag and minimize the different phosphorylation states, the protein was incubated with TEV protease and lambda phosphatase overnight at 4 °C. The following day the protein solution was diluted twice with the same buffer to decrease the salt concentration and then re-concentrated. The sample was then loaded to a MonoQ 5/50 column (Amersham Biosciences, GE Healthcare). After washing the column with 50 mM HEPES pH 7.2, 3 mM DTT, 10% glycerol, a gradient of 0 to 0.5 M NaCl was applied in 50 column volumes. The fractions containing $DAPK1_{1–285}$ were identified by SDS-PAGE and pooled together. In order to remove remaining His-tagged $DAPK1_{1–285}$, the sample was again loaded to Ni-NTA column, but this time the unbound fraction was collected to obtain cleaved $DAPK-1_{1–285}$ (reversed Ni-NTA column). Finally, the sample was applied to a Superdex 26/60 column and eluted in 20 mM Tris pH 7.6, 100 mM NaCl, 1 mM DTT, and 1 mM EDTA. The solution was concentrated to 5 mg/mL for crystallization. The yield was 30 mg of protein per liter of growth culture.

Racemic ruthenium complex **OS4** was added to the protein solution to a final concentration of 0.5 mM. The total concentration of DMSO was 5% which resulted from the inhibitor stock solution. The mixture was incubated on ice for 1 hour followed by centrifugation at 10,000 rpm. Crystallization trials were carried out by sitting drop vapor diffusion at 4 °C with 2 μl protein solution plus 2 μl precipitant solution. Crystals appeared in 100 mM Tris pH 7.6 and 7.5–10% PEG 6000 within 2–3 days. Crystals were cryoprotected in the crystallization buffer supplemented with 25% glycerol and flash frozen in liquid nitrogen.

Expression, purification and crystallization of human GSK3β

GSK3β was expressed and purified as previously described.[23] GSK3β was prepared in 20 mM HEPES pH 7.2, 1 mM DTT, 2 mM $MgCl_2$, 500 mM NaCl, and concentrated to 3 mg/mL for crystallization. Crystals of the apo-protein were obtained at 4 °C in 4 μL hanging drops by mixing 2 μL protein solution with 2 μL precipitant containing 100 mM Tris pH 7.4, 20 % PEG 6000. Crystals grew within 3–5 days. Further optimization of the crystal size was achieved by tuning the diffusion rate by overlaying 400 μL Al's oil (50:50 v/v mixture of Paraffin Oil and Silicon Oil) onto reservoir solution (600μL). The crystals of the native protein were soaked with Λ-**OS1** at a final ligand concentration of 0.5 mM for 6 h in 1% glycerol and 10 % DMSO (in precipitant buffer). Crystals were cryoprotected in the crystallization buffer supplemented with 25% glycerol and flash frozen in liquid nitrogen.

X-ray crystallography

The DAPK1/(*R*)-**OS4** complex was crystallized in spacegroup $P2_12_12_1$ with $\alpha = \beta = \gamma = 90°$ and a = 50.3 Å, b = 77.8 Å and c = 111.3 Å. X-ray data were collected at beamline ID23-2 (14.20 keV, 0.873 Å) of the European Synchrotron Radiation Facility (ESRF, Grenoble, France), at 100 K from a single crystal with a MarMosaic 225 detector system. Data reduction was carried out using XDS and XSCALE.[34] The structure was determined using in-house structural data of DAPK1 (unpublished) by molecular replacement using PHASER[35] of the CCP4[36] package. The Phaser solution with data up to 2.2 Å yielded one molecule per asymmetric unit with z scores of 32.4 for the rotation function and 52.0 for the translation function. Further refinement was carried out with REFMAC5[37] and the model was manually built using COOT[38] at 2.2 Å, which led to 5 outliers (5/274, 1.82%) and 4 residues in allowed regions (7/274, 2.55%) according to the Ramachandran plot. The final statistics reported *R*-factors of R_{work} = 19.8 and R_{free} = 26.0 for the complex with the (*R*)-enantiomer of **OS4** (Table 2). Coordinates and structure factors of DAPK1/(*R*)-**OS4** have been deposited in the protein data bank under the accession code 2YAK.

The GSK3β/Λ-**OS1** complex was crystallized in spacegroup $P2_12_12_1$ with $\alpha = \beta = \gamma = 90°$ and a = 83.32 Å, b = 84.30 Å and c = 178.12 Å. X-ray data were collected at beamline ID23-2 (14.20 keV, 0.873 Å) of the European Synchrotron Radiation Facility (ESRF, Grenoble, France), at 100 K from a single crystal with a MarMosaic 225 detector system. Indexing and integration were carried out using MOSFLM[39] and scaling was performed with SCALA[40]. Initial phases were calculated by molecular replacement with PHASER[34] using a known model of GSK3β (PDB code 2JLD).[23] The ligand was modeled into the experimental density and building was completed manually with COOT.[38] Refinement was carried out in REFMAC5.[37] Thermal motions were analyzed using TLSMD[41] and hydrogen atoms were included in late refinement cycles. The final statistics reported *R*-factors of R_{work} = 20.4 and R_{free} = 24.9 for the complex with L-**OS1** (Table 2). Coordinates and structure factors of GSK3β/Λ-**OS1** have been deposited in the protein data bank under the accession code 3PUP.

Computational methods

The geometry optimization and frequency calculations of Λ-**OS1**, Λ-**OS2**, and single enantiomers of **OS3–OS6** were carried out using the BP86[42,43] functional in conjunction with the def2-SVP[44] basis set as implemented in Gaussian03[45]. The CPCM-SCRF[46,47] calculations were performed to address solvation effects. The dielectric constant of water (ε=78.39) was utilized in order to simulate the solvent environment. In CPCM, the choice of cavities is important, because the computed energies and properties depend on the cavity size. In this study, the united atom topological model (UAO)[48] was used, which uses radii from the UFF[49] force field. The energy difference between bent and linear coordinated NCS ligand in **OS4** was calculated in methanol (ε=32.63) and acetone (ε=20.70) by using the

M05[50,51] functional and the CPCM method in conjunction with the def2-SVP basis set at CPCM and BP86/def2-SVP/CPCM level. Molecular electrostatic potential surfaces were created with GaussView 5.0.8. See Supporting Information for more information.

Supplementary Material

Refer to Web version on PubMed Central for supplementary material.

Acknowledgments

References

1. Schreiber SL. Bioorg. Med. Chem. 1998; 6:1127–1152. [PubMed: 9784856]

2. Tolliday N, Clemons PA, Ferraiolo P, Koehler AN, Lewis TA, Li X, Schreiber SL, Gerhard DS, Eliasof S. Cancer Res. 2006; 66:8935–8942. [PubMed: 16982730]

3. Oprea TI, et al. Nature Chem. Biol. 2009; 5:441–447. [PubMed: 19536101]

4. Frye SV. Nature. 2010; 6:159–161.

5. International Human Genome Sequencing Consortium. Nature. 2004; 431:931–945. [PubMed: 15496913]

6. Bain J, McLauchlan H, Elliott M, Cohen P. Biochem. J. 2003; 371:199–204. [PubMed: 12534346]

7. Knight ZA, Shokat KM. Chem. Biol. 2005; 12:621–637. [PubMed: 15975507]

8. Fabian MA, et al. Nat. Biotechnol. 2005; 23:329–336. [PubMed: 15711537]

9. Fedorov O, Marsden B, Pogacic V, Rellos P, Müller S, Bullock AN, Schwaller J, Sundström M, Knapp S. Proc. Natl. Acad. Sci. USA. 2007; 104:20523–20528. [PubMed: 18077363]

10. Peters EC, Gray NS. ACS Chem. Biol. 2007; 2:661–664. [PubMed: 18041816]

11. Karaman MW, et al. Nat. Biotechnol. 2008; 26:127–132. [PubMed: 18183025]

12. An exception are reactive inhibitors that can form specific covalent bonds within the target active site. See, for example: a.) Cohen MS, Zhang C, Shokat KM, Taunton J. Science. 2005; 308:1318–1321. [PubMed: 15919995] ; b.) Singh J, Petter RC, Kluge AF. Curr. Opin. Chem. Biol. 2010; 14:475–480. [PubMed: 20609616] ; c.) Hagel M, Niu D, St. Martin T, Sheets MP, Qiao L, Bernard H, Karp RM, Zhu Z, Labenski MT, Chaturvedi P, Nacht M, Westlin WF, Petter RC, Singh J. Nat. Chem. Biol. 2011; 7:22–24. [PubMed: 21113170]

13. Meggers E. Angew. Chem. Int. Ed. 2011; 50:2442–2448.

14. Meggers E, Atilla-Gokcumen GE, Bregman H, Maksimoska J, Mulcahy SP, Pagano N, Williams DS. Synlett. 2007; 8:1177–1189.

15. Bailor JC. J. Chem. Ed. 1957; 34:334–338.

16. a.) Meggers E. Curr. Opin. Chem. Biol. 2007; 11:287–292. [PubMed: 17548234] b.) Meggers E. Chem. Commun. 2009:1001–1010.c.) Davies CL, Dux EL, Duhme-Klair A-K. Dalton Trans. 2009:10141–10154. [PubMed: 19921045]

17. Gasser G, Ott I, Metzler-Nolte N. J. Med. Chem. 2011; 54:3–25.

18. Bregman H, Carroll PJ, Meggers E. J. Am. Chem. Soc. 2006; 128:877–884. [PubMed: 16417378]

19. Maksimoska J, Feng L, Harms K, Yi C, Kissil J, Marmorstein R, Meggers E. J. Am. Chem. Soc. 2008; 130:15764–15765. [PubMed: 18973295]

20. Wilbuer A, Vlecken DH, Schmitz DJ, Kräling K, Harms K, Bagowski CP, Meggers E. Angew. Chem. Int. Ed. 2010; 49:3839–3842.

21. Dobson CM. Nature. 2004; 432:824–828. [PubMed: 15602547]

22. Xie P, Streu C, Qin J, Bregman H, Pagano N, Meggers E, Marmorstein R. Biochemistry. 2009; 48:5187–5198. [PubMed: 19371126]

23. Atilla-Gokcumen GE, Pagano N, Streu C, Maksimoska J, Filippakopoulos P, Knapp S, Meggers E. ChemBioChem. 2008; 9:2933–2936. [PubMed: 19035373]

24. Knighton DR, Zheng JH, Ten Eyck LF, Ashford VA, Xuong NH, Taylor SS, Sowadski JM. Science. 1991; 253:407–414. [PubMed: 1862342]

25. Bertrand JA, Thieffine S, Vulpetti A, Cristiani C, Valsasina B, Knapp S, Kalisz HM, Flocco M. J. Mol. Biol. 2003; 333:393–407. [PubMed: 14529625]

26. Meijer L, et al. Chem. Biol. 2003; 10:1255–1266. [PubMed: 14700633]

27. Hemmer W, McGlone M, Tsigelny I, Taylor SS. J. Biol. Chem. 1997; 272:16946–16954. [PubMed: 9202006]

28. Tsigelny I, Greenberg JP, Cox S, Nichols WL, Taylor SS, Ten Eyck LF. Biopolymers. 1999; 50:513–524. [PubMed: 10479734]

29. Atilla-Gokcumen GE, Di Costanzo L, Meggers E. J. Biol. Inorg. Chem. 2011; 16:45–50. [PubMed: 20821241]

30. Debreczeni JÉ, Bullock AN, Atilla GE, Williams DS, Bregman H, Knapp S, Meggers E. Angew. Chem. Int. Ed. 2006; 45:1580–1585.

31. Tereshko V, Teplova M, Brunzelle J, Watterson DM, Egli M. Nature Struct. Biol. 2001; 8:899–907. [PubMed: 11573098]

32. Clemons PA, Bodycombe NE, Carrinski HA, Wilson JA, Shamji AF, Wagner BK, Koehler AN, Schreiber SL. Proc. Nat. Acad. Sci. USA. 2010; 107:18787–18792. [PubMed: 20956335]

33. It is worth noting that the octasporine metal complexes display lower IC_{50} values compared to their respective pyridocarbazole ligands: Λ-**OS1**/GSK3α: 8890-fold, Λ-**OS2**/PAK1: not determined due to insolubility of the corresponding pyridocarbazole ligand, **OS3**/Pim1: 60-fold, **OS4**/DAPK1: >15000-fold, **OS5**/MLCK: >6800-fold, **OS6**/FLT4: 1.8-fold. See Supporting Information for more details.

34. Kabsch W. J. Appl. Cryst. 1993; 26:795–800.

35. McCoy AJ, Grosse-Kunstleve RW, Adams PD, Winn MD, Storoni LC, Read RJ. J. Appl. Cryst. 2007; 40:658–674. [PubMed: 19461840]

36. Collaborative computational project, number 4. The CCP4 suite: programs for protein crystallography. Acta Cryst. 1994; D50:760–763.

37. Murshudov GN, Vagin AA, Dodson EJ. Acta Cryst. 1997; D53:240–255.

38. Emsley P, Lohkamp B, Scott WG, Cowtan K. Acta Cryst. 2010; D66:486–501.

39. MOSFLM. v.7.01. MRC Laboratory of Molecular Biology; Cambridge: 2007.

40. SCALA - scale together multiple observations of reflections. v.3.3.0. MRC Laboratory of Molecular Biology; Cambridge: 2007.

41. Painter J, Merritt EA. Acta Cryst. 2006; D62:439–450.

42. Becke AD. Phys. Rev. A. 1988; 38:3098–3100. [PubMed: 9900728]

43. Perdew JP. Phys. Rev. B. 1986; 33:8822–8824.

44. Schäfer A, Horn H, Ahlrichs R. J. Chem. Phys. 1992; 97:2571–2577.

45. Frisch, MJ., et al. Gaussian 03, Revision E.01. Gaussian, Inc.; Wallingford CT: 2004.

46. Barone V, Cossi M. J. Phys. Chem. A. 1998; 102:1995–2001.

47. Cossi M, Rega N, Scalmani G, Barone V. J. Comp. Chem. 2003; 24:669–681. [PubMed: 12666158]

48. Cossi M, Barone V, Cammi R, Tomasi J. Chem. Phys. Lett. 1996; 255:327–335.

49. Rappe AK, Casewit CJ, Colwell KS, Goddard WA III, Skiff WM. J. Am. Chem. Soc. 1992; 114:10024–10035.

50. Zhao Y, Schultz NE, Truhlar DG. J. Chem. Theory Comput. 2006; 2:364–382.

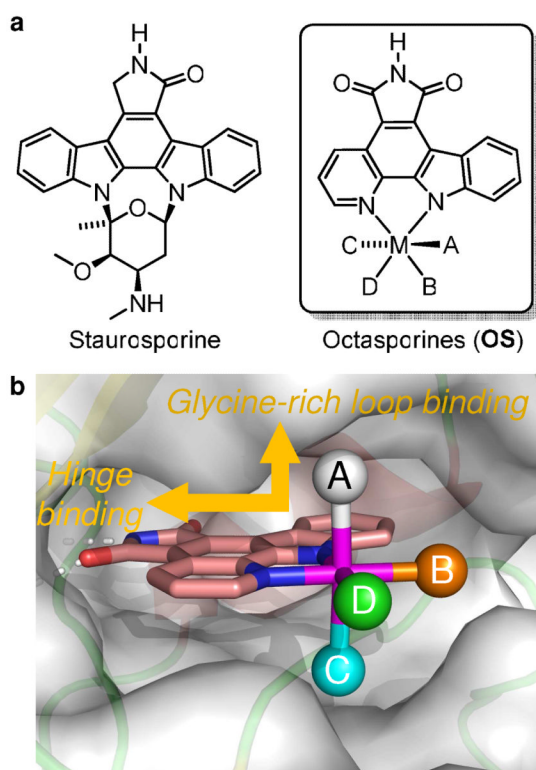51. Zhao Y, Truhlar DG. Acc. Chem. Res. 2008; 41:157–167. [PubMed: 18186612]

Figure 1.
Octasporines as protein kinase inhibitors. (a) Staurosporine as a structural inspiration for the design of metal-based protein kinase inhibitors. (b) Binding of the octahedral pyridocarbazole metal complex scaffold to the ATP-binding site of a protein kinase. The metal center in combination with the coordinating ligands A-D controls the shape and functional group presentation of the molecular scaffold. A unique aspect of this octahedral scaffold is that the orthogonal orientation of the pyridocarbazole heterocycle and the ligand A simultaneously enable efficient interactions with both the hinge region and the glycine-rich loop.
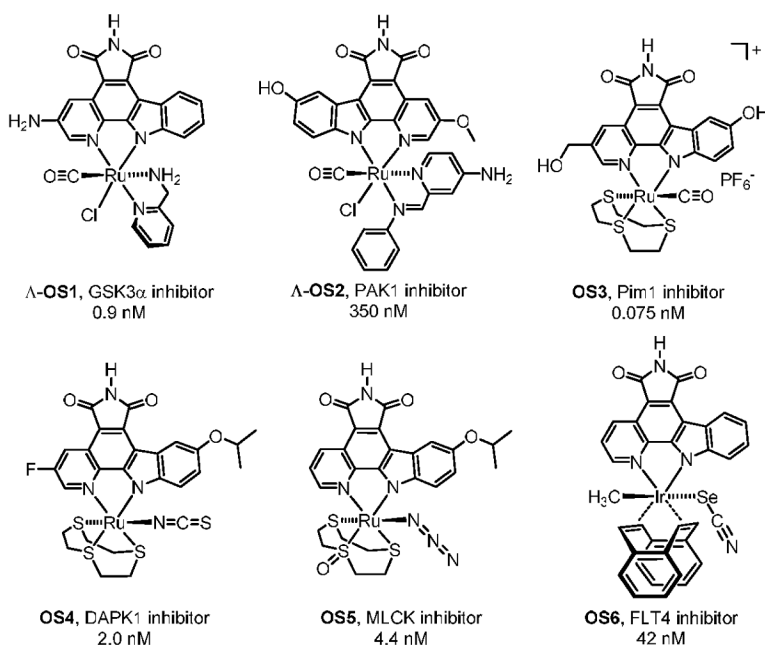
Figure 2.
Molecular structures of highly selective octasporine protein kinase inhibitors developed in this study. The compounds Λ-**OS1** and Λ-**OS2** are single enantiomers, whereas **OS3–OS6** are racemic mixtures (only one enantiomer shown). IC$_{50}$ values were determined in the presence of 100 μM ATP.
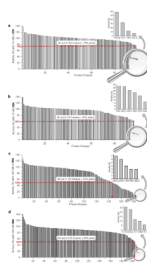
Figure 3.
Screening of compounds Λ-**OS1**, **OS4**, **OS5**, and **OS6** against panels of human wild type protein kinases. Each bar represents the activity of one individual protein kinase. Protein kinases in each panel (Millipore KinaseProfiler) were solely selected on the basis that their concentration was equal to or lower than the concentration used of the screened compound. All assays were performed with 10 μM ATP. Data shown represent the mean value of duplicate measurements. (a) GSK3α inhibitor Λ-**OS1** tested at a concentration of 10 nM against 102 protein kinases. (b) DAPK1 inhibitor **OS4** tested at a concentration of 10 nM against 102 protein kinases. (c) MLCK inhibitor **OS5** tested at a concentration of 100 nM against a panel of 191 protein kinases. (d) FLT4 inhibitor **OS6** tested at a concentration of 300 nM against a panel of 215 protein kinases. See Supporting Information for more details.
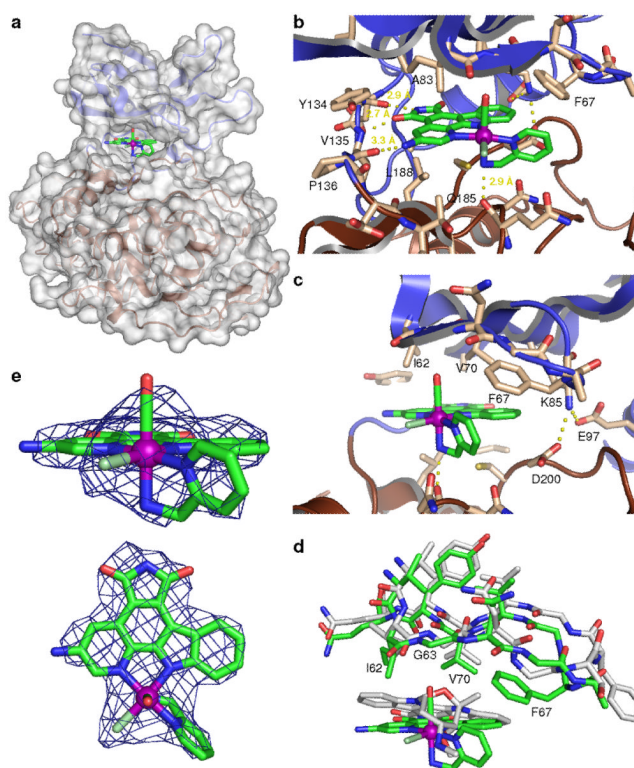
Figure 4.
Crystal structure of GSK3b with Λ-**OS1**. (a) Overall structure with Λ-**OS1** bound to the ATP-binding site. (b,c) Interactions of Λ-**OS1** within the active site of GSK3β. Labeled amino acids are involved in hydrogen bonds to the ruthenium complex. (d) Binding position of Λ-**OS1** (the carbon atoms of the glycine-rich loop are shown in green) and staurosporine (the carbon atoms of the glycine-rich loop are shown in grey, PDB code 1Q3D) relative to the position of the glycine-rich loop of GSK3β. (e) Calculated $2F_{obs}$-F_{calc} difference electron density map of the inhibitor contoured at 2 σ.
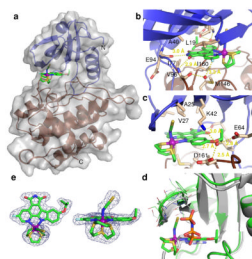
Figure 5.
Cocrystal structure of DAPK1 with (*R*)-**OS4**. (a) Overall fold with (*R*)-**OS4** bound to the ATP-binding site. (b,c) (*R*)-**OS4** stabilization occurs via hydrogen bonds and hydrophobic contacts with various protein residues. (d) DAPK1/(*R*)-**OS4** complex superimposed with the co-crystal structure of DAPK1 and AMPPnP shown in grey (PDB code 1JKL). (e) $2F_{obs}$-F_{calc} difference electron density map of the inhibitor contoured at 1 σ. Note: The absolute configuration at the ruthenium was assigned according to the Cahn-Ingold-Prelog rules treating the complex as being pseudo-tetrahedral with the 1,4,7-trithiacyclononane being formally regarded as a single substituent, with the priority order of the substituents being 1,4,7-trithiacyclononane > pyridine [N(C,C,C)] > NCS > indole [N(C,C,lone pair)].
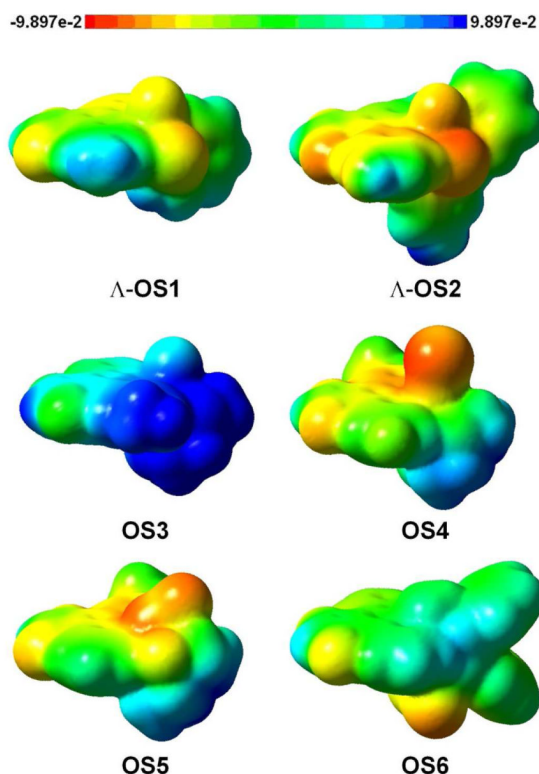
Figure 6.
Molecular electrostatic potential surfaces of the octasporine inhibitors. In this diagram, red color represents negative electrostatic potential, green color represents zero, and blue color represents positive electrostatic potential in hartrees. Note that the large regions of positive electrostatic potential in **OS3** is due to the monocationic nature of the metal complex. The molecular electrostatic potential surface of **OS3** does not include the PF_6 counterion. The molecular electrostatic potential surface of **OS3** including the associated PF_6 counterion can be found in the Supporting Information. The metal complex geometries were determined from DFT calculations at the BP86/def2-SVP/CPCM level under consideration of water solvation effects (see Experimental Part and Supporting Information).
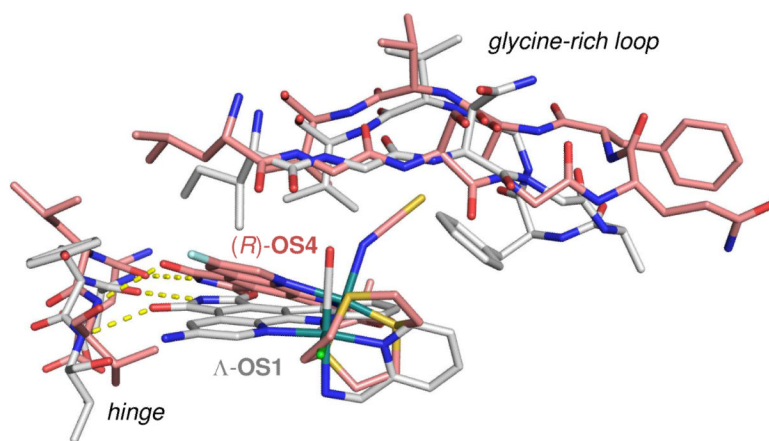
Figure 7.
Superimposed structures GSK3b/Λ-**OS1** (carbon atoms in grey) and DAPK1/(*R*)-**OS4** (carbon atoms in pink), revealing the relative binding positions with the hinge region and the glycine-rich loop.

Table 1

IC$_{50}$ data (nM) for octahedral kinase inhibitors at 100 μM ATP.[a]

	GSK3α	PAK1	PIM1	DAPK1	MLCK	FLT4
Λ-**OS1**	0.9	>100000	14	22800	22	1180
Λ-**OS2**	2000	350	1570	>30000	24300	2300
OS3	20	82	0.075	315	2.2	29
OS4	>100000	>100000	169	2.0	25	163
OS5	31000	>100000	435	113	4.4	48
OS6	3900	10000	333	>100000	>30000	42

[a]IC$_{50}$ data were obtained by phosphorylation of substrates with [γ-^{33}P]ATP and 100 μM ATP in the presence of different concentrations of octasporine kinase inhibitors. See Supporting Information for standard deviations.

Table 2

X-ray data collection, processing and refinement statistics.

	DAPK1/(*R*)-OS4	GSK3β/Λ-OS1
	Data collection and processing	
Space Group	P2$_1$2$_1$2$_1$	P2$_1$2$_1$2$_1$
Cell dimensions:		
a, b, c (Å)	50.30, 77.80, 111.30	83.32, 84.30, 178.12
α, β, γ(°)	90.00, 90.00, 90.00	90.00, 90.00, 90.00
Resolution (Å)[*]	24.53 – 2.20 (2.26 – 2.20)	49.33 – 2.99 (3.15 – 2.99)
Unique observations[*]	21538 (3151)	25373 (3651)
Completeness[*] (%)	95.1 (96.8)	97.3 (97.7)
Redundancy[*]	5.0 (4.6)	5.0 (4.8)
R$_{merge}$	0.098 (0.815)	0.186 (0.772)
I/ σI[*]	13.9 (1.8)	6.3 (2.0)
	Refinement	
Resolution	2.20	2.99
R$_{work}$/*R*$_{free}$	19.8 / 26.0	20.4 / 24.9
Number of atoms (Protein/other/water)	2234 / 40 / 108	5324 / 70 / -
B-factors(Å^2) (protein/other/water)	32.5 / 30.2 / 36.0	52.0 / 48.0/ -
R.m.s deviations		
Bond lengths (Å)	0.021	0.016
Bond angles (°)	1.78	1.52
Ramachandran plot:		
Favoured (%)	95.62	94.42
Allowed (%)	2.55	4.55
Disallowed (%)	1.82	1.03

[*] Values in parentheses correspond to the highest resolution shell.

Table 3

Conditions for IC$_{50}$ value determinations.

Kinase	Kinase conc. (nM)	Substrate	Substrate conc. (μM)	[γ-^{33}P]ATP conc. (μCi/μL)	Incubation time (min)
GSK3α	1.8[a]	PGSP-2	20	0.05	45
PAK1	0.2	MBP	10	0.06	45
PIM1	1.6[b]	S6 peptide	50	0.04	30[c]
DAPK1	1.0	ZIP peptide	62.5	0.08	30
MLCK	4.6[d]	ZIP peptide	62.5	0.1	30[c]
FLT4	8.8	JAK3tide	100	0.1	180
FLT1	6.1	IGF-IRtide	100	0.1	180
ZIPK	10	ZIP peptide	62.5	0.1	30
RET	2.5	IGF-IRtide	100	0.1	30

[a] Concentration of GSK3α was 0.9 nM for Λ-**OS1**.

[b] Concentration of PIM1 was 64 pM for **OS3**.

[c] Incubation time was 45 min for **OS3**.

[d] Concentration of MLCK was 1.8 nM for **OS3**.